.

High speed adaptive liquid microlens array

C. U. Murade, D. van der Ende, F. Mugele*

Physics of Complex Fluids, MESA+ Institute for Nanotechnology, University of Twente, 7521 AE, Enschede, The Netherlands.
**f.mugele@utwente.nl*

Abstract: Liquid microlenses are attractive for adaptive optics because they offer the potential for both high speed actuation and parallelization into large arrays. Yet, in conventional designs, resonances of the liquid and the complexity of driving mechanisms and/or the device architecture have hampered a successful integration of both aspects. Here we present an array of up to 100 microlenses with synchronous modulation of the focal length at frequencies beyond 1 kHz using electrowetting. Our novel concept combines pinned contact lines at the edge of each microlens with an electrowetting controlled regulation of the pressure that actuates all microlenses in parallel. This design enables the development of various shapes of microlenses. The design presented here has potential applications in rapid parallel optical switches, artificial compound eye and three dimensional imaging.

OCIS codes: (000.4930) Other topics of general interest; (080.3630) Lenses; (110.1080) Active or adaptive optics; (230.2090) Electro-optical devices; (230.0230) Optical devices.

References and links

1. C. V. Brown, G. G. Wells, M. I. Newton, and G. McHale, "Voltage-programmable liquid optical interface," Nat. Photonics **3**, 403-405 (2009).
2. D. Erickson, D. Sinton, and D. Psaltis, "Optofluidics for energy applications," Nat. Photonics **5**, 583-590 (2011).
3. L. Dong, A. K. Agarwal, D. J. Beebe, and H. R. Jiang, "Adaptive liquid microlenses activated by stimuli-responsive hydrogels," Nature **442**, 551-554 (2006).
4. C. A. Lopez and A. H. Hirsa, "Fast focusing using a pinned-contact oscillating liquid lens," Nat. Photonics **2**, 610-613 (2008).
5. T. Krupenkin and J. A. Taylor, "Reverse electrowetting as a new approach to high-power energy harvesting," Nat. Commun. **2**, 101038 (2011).
6. H. Gu, C. U. Murade, M. H. G. Duits, and F. Mugele, "A microfluidic platform for on-demand formation and merging of microdroplets using electric control," Biomicrofluidics **5**, 011101 (2011).
7. U. Levy and R. Shamai, "Tunable optofluidic devices," Microfluid Nanofluid **4**, 97-105 (2008).
8. P. M. Moran, S. Dharmatilleke, A. H. Khaw, K. W. Tan, M. L. Chan, and I. Rodriguez, "Fluidic lenses with variable focal length," Appl. Phys. Lett. **88**, 041120 (2006).
9. N. R. Smith, L. L. Hou, J. L. Zhang, and J. Heikenfeld, "Fabrication and Demonstration of Electrowetting Liquid Lens Arrays," J. Disp. Technol. **5**, 411-413 (2009).
10. B. Berge and J. Peseux, "Variable focal lens controlled by an external voltage: An application of electrowetting," Eur. Phys. J. E **3**, 159-163 (2000).
11. S. Kuiper and B. H. W. Hendriks, "Variable-focus liquid lens for miniature cameras," Appl. Phys. Lett. **85**, 1128-1130 (2004).
12. N. R. Smith, D. C. Abeysinghe, J. W. Haus, and J. Heikenfeld, "Agile wide-angle beam steering with electrowetting microprisms," Opt. Express **14**, 6557-6563 (2006).
13. L. Miccio, A. Finizio, S. Grilli, V. Vespini, M. Paturzo, S. De Nicola, and P. Ferraro, "Tunable liquid microlens arrays in electrode-less configuration and their accurate characterization by interference microscopy," Opt. Express **17**, 2487-2499 (2009).
14. C. U. Murade, J. M. Oh, D. van den Ende, and F. Mugele, "Electrowetting driven optical switch and tunable aperture," Opt. Express **19**, 15525-15531 (2011).
15. J. M. Oh, S. H. Ko, and K. H. Kang, "Analysis of electrowetting-driven spreading of a drop in air," Phys. Fluids **22**, 032002 (2010).

16. A. Staicu and F. Mugele, "Electrowetting-induced oil film entrapment and instability," Phys. Rev. Lett. **97**, 167801 (2006).
17. F. Mugele and J. C. Baret, "Electrowetting: From basics to applications," J. Phys-Condens Mat. **17**, R705-R774 (2005).
18. F. Li and F. Mugele, "How to make sticky surfaces slippery: Contact angle hysteresis in electrowetting with alternating voltage," Appl. Phys. Lett. **92**, 244108 (2008).
19. D. J. C. M. 't Mannetje, C. U. Murade, D. van den Ende, and F. Mugele, "Electrically assisted drop sliding on inclined planes, " Appl. Phys. Lett. **98**, 014102 (2011).
20. E. A. Theisen, M. J. Vogel, C. A. Lopez, A. H. Hirsa, and P. H. Steen, "Capillary dynamics of coupled spherical-cap droplets," J. Fluid Mech. **580**, 495-505 (2007).
21. H. Rathgen, K. Sugiyama, C. D. Ohl, D. Lohse, and F. Mugele, "Nanometer-resolved collective micromeniscus oscillations through optical diffraction," Phys. Rev. Lett. **99**, 214501 (2007).
22. J. M. Oh, D. Legendre, and F. Mugele, "Shaken not stirred -On internal flow patterns in oscillating sessile drops," Europhys. Lett. **98**, 34003 (2012).
23. I. Roghair, C. U. Murade, J. M. Oh, D. Langevin, D. van den Ende and F. Mugele (to be submitted).
24. F. Okano, H. Hoshino, J. Arai, and I. Yuyama, "Real-time pickup method for a three-dimensional image based on integral photography," Appl. Optics **36**, 1598-1603 (1997).
25. Like electrowetting, intergral photography was pioneered by the 1908 Nobel prize winner Gabriel Lippmann: Lippmann, G., J. Phys. 7, 821-825, (1908).

1. Introduction

Adaptive liquid lenses belong to the rapidly growing class of optofluidic devices that combine the control of fluids and light on the micrometer scale to enable novel applications for optical sensing, manipulation, imaging and displaying [1-6]. Various concepts of adaptive lenses have been developed in recent years to match the increasing demand for a variety of applications including mobile phones, surgical endoscopes, security cameras and DVD players [7]. Next to liquid crystal-based approaches novel liquid lenses in various configurations have been proposed using responsive hydrogels [3], piezoelectricity [8], acoustics [4] and Electrowetting (EW) [9-14] as actuation mechanisms. The latter is particularly useful for the design of compact and robust devices combining simple electrical driving with actuation speeds exceeding video rate for sub-millimetric lenses. A disadvantage limiting the actuation speed and the accuracy of conventional design of EW lenses, however, is the motion of the three-phase contact line, i.e. the edge of the lens, as electric forces are applied to change the focal length. The electric forces pulling on the contact line couple directly to the shape modes of the liquid surface [15] and thereby give rise to distortions of the lens at high actuation frequencies. Here we introduce an EW-based microlens array that avoids the complications mentioned above and therefore reaches high speed actuation of up to 100 microlenses. An additional advantage of our design is that all microlenses are actuated simultaneously by one common electrode outside the optical path. This avoids detrimental effects of minor lens-to-lens variations due to minor fabrication tolerances or long term stability.

2. Microlens array

The design of our EW based microlens array consists of a sandwich structure with a drop of conducting liquid between two parallel plates at a distance h (Fig. 1). The top plate features an array of aperture holes through which the liquid protrudes and forms spherical cap-shaped microlenses with contact lines pinned to the edges of the aperture. The electrowetting substrate at the bottom surface of the device is prepared by dip coating a Teflon AF film with a thickness of $d \approx 2\text{-}3\mu m$ onto a glass substrate that is covered with 30 nm thin transparent electrode made from Indium Tin Oxide (ITO). The Teflon film is impregnated prior with silicone oil to assembling the device in order to reduce the contact angle hysteresis to 1-2°. By functionalizing the bottom surface for EW we can control the pressure in the liquid phase using the applied voltage. This novel concept greatly improves the performance of current designs of EW-driven liquid lenses. In particular, the use of pinned contact lines eliminates the effect of contact angle hysteresis and/or oil entrapment [16] at the moving contact line that compromise the performance of conventional EW-lenses at high actuation speeds. This aspect is particularly important for microlenses, where imperfections on the substrate surface have an even more detrimental effect than for millimeter-sized liquid lenses. Moreover, the geometric separation of the lensing effect at each aperture and the EW-induced pressure variation in the reservoir drop allow for very simple parallelization that eliminates the need for actuation electrodes at each microlens [12]. This tremendously reduces the complexity of the manufacturing process and results in simple robust lens arrays. Together, these benefits enable the first demonstration of a truly high-speed adaptive liquid microlens array with modulation frequencies beyond 1 kHz.

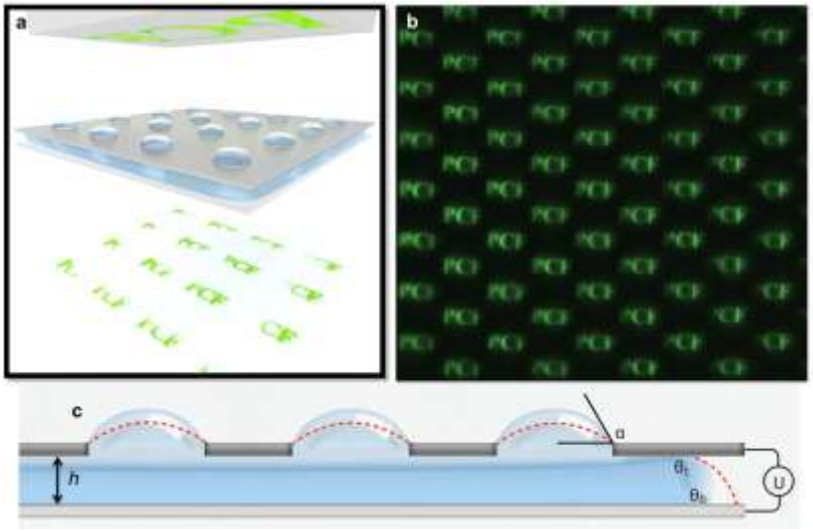

Fig. 1. Microlens array. (a) Schematics of the microlens array, object PCF is placed at a finite distance from the microlens array, the object is illuminated from the top. (b) Image acquired by the microlens array. (c) Side view of the microlens array, the water meniscus is pinned at the lens aperture with lens angle α, as voltage is applied across the bottom electrowetting plate and the top plate (lens aperture) the contact angle of water at the bottom substrate changes which also changes the curvature of the lens meniscus both denoted by dotted red line.

The basic operation principle of the microlens array is illustrated in Fig. 1. In equilibrium, the pressure inside the liquid is constant and hence the curvatures of the surface of all liquid microlenses are equal to the curvature κ at the edge of the sandwiched reservoir drop. For a large reservoir drop, κ is determined by h and by the contact angles θ_t and θ_b on the top and bottom plate, respectively: $\kappa \approx (\cos\theta_t + \cos\theta_b)/h$. For freely moving contact lines on both surfaces, θ_t is given by Young's angle θ_Y and θ_b by the voltage-dependent contact angle $\theta(U)$ following the EW Eq. [17]

$$\cos\theta(U) = \cos\theta_Y + \frac{\varepsilon_0 \varepsilon_d U^2}{2d\gamma} = \cos\theta_Y + \eta \qquad (1)$$

Here, ε_d and d is dielectric constant and thickness of the insulating layer, ε_0 is the dielectric permittivity of vacuum, U is the applied voltage and η is the dimensionless EW number. The reduction of $\theta(U)$ with increasing U reduces the lens angle α (see Fig. 1(c)) and thereby the curvature of the liquid surface and hence increases the focal length f. EW thus indirectly controls the focal length by regulating the pressure in the liquid phase. Combining simple geometric relations and the lens maker formula, one obtains the focal length f as

$$f = -\frac{2h}{\Delta n(2\cos\theta_Y + \eta)} \qquad (2)$$

($\Delta n = n/n_{air}$-1). For typical values of $\theta_Y = 120°$, $\eta_{max} = 0.7$ and $\Delta n = 0.33$ this yields a range of accessible focal lengths of $f \approx (6 \ldots 20) \times h$. In our devices, we use h = 0.45 mm and 0.06 – 0.07 mm for the single lens and for the lens array, respectively.

3. Characterization of individual lens

We demonstrate the basic functionality of the system for a single macroscopic lens with an aperture diameter of 1.2 mm and a plate spacing h=0.45 mm. This configuration allows for a simultaneous characterization of the optical properties of the lens as well as the morphology of the fluid. Figure 2 shows the variation of the lens angle α and the resulting focal length f with increasing voltage (see also supplementary Information Movie 1).

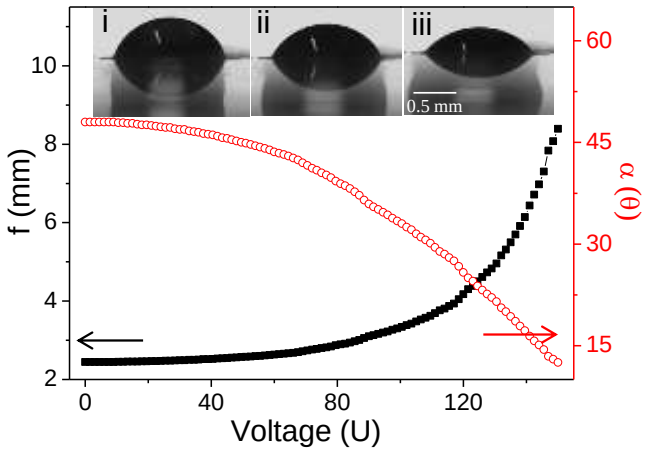

Fig. 2 Focal length and lens angle α of single lens (diameter: 1.2mm) vs. applied voltage. inset: side view images of the lens and the reservoir drop from low to high voltage (left to right). The bottom half of the lenses are reflections in the top plate.

Integrating this lens into a custom-built microscope, we can scan the focal plane to image objects at variable distance from the objective. The liquid lens is placed in front of a microscope objective (10x, 0.3 NA) and the images created by the liquid lens are projected onto the CCD detector by the microscope objective (Fig. 3(b)). Figure 3 demonstrates this for a sample consisting of colloidal particles (diameter = 15 µm) deposited onto the top and bottom side of a microscope cover slip with a thickness of 170 µm. By varying the applied voltage we scan the focal plane of the lens and focus on either the top or the bottom surface (supplementary information Movie 2). Such relatively large systems can thus act as a fast and simple-to-use tunable optical element with potential applications for scanning confocal imaging systems.

To quantify the focusing behavior, we calculate the sharpness *S* of the images as a function of time for the two object planes. We define *S* as the maximum of the gradient of the intensity along a cross section through one of the particles in the images normalized by its maximum value in a given image sequence. For the data in Fig. 3 the scan range of the focal plane is somewhat larger than the spacing of the top and the bottom surface. Hence the colloidal particles on the top surface (blue curve in Fig. 3(c)) come into focus twice during each oscillation cycle whereas the bottom surface (red curve) comes into focus only once. Images of the quality presented here can be obtained up to a modulation frequency of approximately 70 Hz. Using high speed image grabbing synchronized with the oscillation of the lens as proposed by Lopez and Hirsa [4], this allows for high speed scanning of a three-dimensional sample in the z-direction. For the present macroscopic lens, higher eigenmodes of the oscillating drop surface deteriorate the image quality for modulation frequencies of 100 Hz and higher. Substantially higher modulation frequencies in the kHz range can be achieved by miniaturization, as we will show in the next paragraph for arrays of microlenses. Next to simple spherical lenses, the design principle of EW-driven lenses with pinned contact lines lends itself to other, in principle arbitrary, geometries of the lens aperture. In the supplementary information we demonstrate a tunable line focus obtained with a cylindrical lens (supplementary information Movie 3).

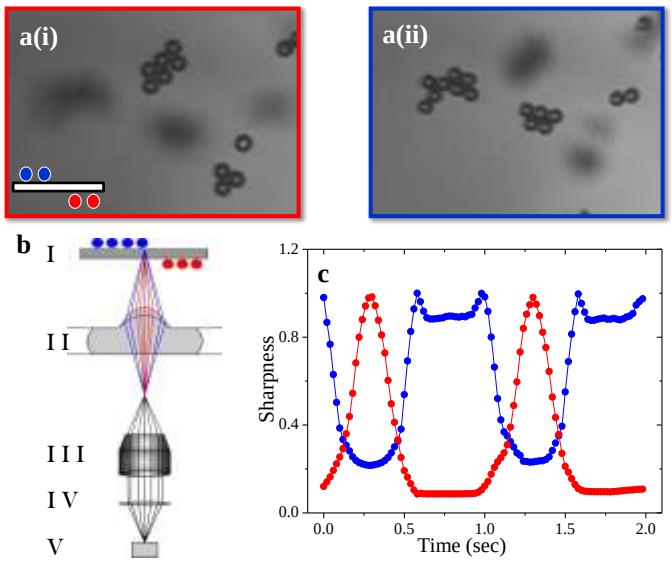

Fig. 3 Scanning imaging system. (a) Images of polystyrene particles (diameter 15 µm) placed on both side of a 170 µm thick cover slip focusing on the bottom (i) and top (ii) side, respectively (individual imaging lens; diameter: 1.2mm). (b) Schematics of the single liquid lens imaging the beads, I – V presents sample, liquid lens, microscope objective, lens and CCD camera respectively. (c) Sharpness of the imaged beads (bottom and top) as function of time upon ramping up and down the applied voltage.

4. Integration into lens array

The most attractive aspect of the present liquid lens concept is its straightforward capability for miniaturization and parallelization into arrays of identical microlenses. Such an array is achieved by replacing the top plate with the single millimeter-sized hole as in Fig. 2 by a surface containing an array of small apertures (see Fig. 1). Since the microlenses are all connected to the same reservoir drop, changing the pressure in the latter simultaneously changes the focal length of all microlenses (supplementary information Movie 4). In contrast to an array design based on the parallelization of conventional EW-lenses, which requires EW-actuation for each individual lens, the present approach thus requires only a single actuation electrode. This renders the present design particularly fault tolerant and allows for a simple and robust production process.

Figure 4(a) shows a slanted top view of such a hexagonal array of microcircular lenses with a diameter of 200 µm. The array top plate consists of a simple grid for transmission electron microscopy (TEM) mounted at a fixed height above the bottom electrode using polymeric spacers. Figure 4(b) shows snapshots of an object recorded with a few adjacent microlenses upon varying the applied voltage. Since the voltage applied to the single electrode simultaneously modulates the pressure for all microlenses the variation of their focal lengths is perfectly in phase as demonstrated by the perfectly synchronous variation of the sharpness for several adjacent lenses in Fig. 4(c).

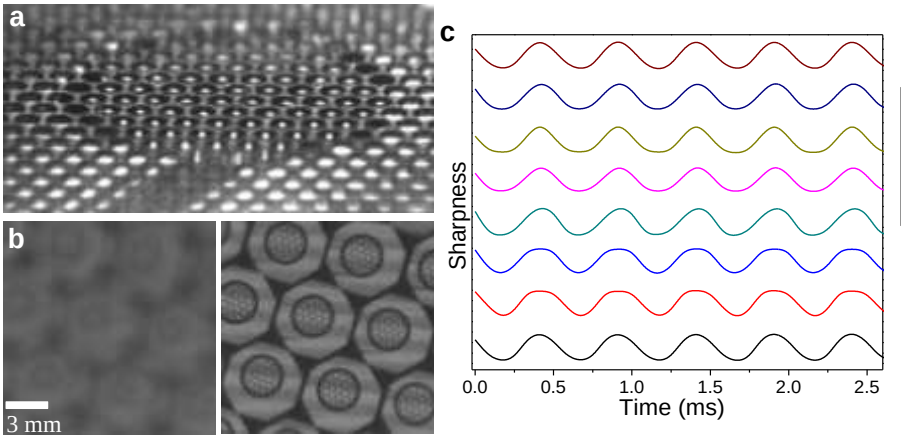

Fig. 4 Synchronized microlens array. (a) Slanted view of the microlens array. (b) Imaging ability of the microlens array. (c) Sharpness plot of the images acquired by each microlens as function of time, indicating the synchronized modulation of the microlens array.

Thanks to their small size, the microlenses display a fast response time. Interestingly, the response of the lens depends strongly on the specific waveform used for excitation. While actuation with conventional AC voltage allows for focus modulation of a few hundred Hz, we can achieve modulation frequencies up to 3kHz for the same lens array by driving the lens with a high frequency (10 kHz) AC carrier frequency with amplitude modulation. Figure 5(a) shows a series of snapshots obtained from a single microlens obtained with the latter actuation waveform (supplementary information Movie 5). In Fig. 5(b), we plot the amplitude of the intensity variation obtained by modulating the lens with the two different actuation modes, AC (black squares) and amplitude modulation (red circles). (This signal is equivalent to measuring the variation of the intensity passing a pinhole as the focus of the lens is scanned along the optical axis through the lens.) Clearly, the intensity modulation with pure AC actuation decays dramatically between 500Hz and 1kHz, whereas the modulation obtained with amplitude modulation is largely constant up to 3kHz. We attribute this different behavior to the efficient depinning of the contact line at the carrier frequency that is known to reduce the effective contact angle hysteresis and to facilitate contact line motion [18, 19]. Figure 5(c) presents the modulation of the sharpness for a single microlens with an aperture diameter of 75 µm. This microlens can be modulated up to 20 kHz, consistent with estimates based on the eigenfrequency hemispherical drops of this size [4].

For substantially higher driving frequencies hydrodynamic coupling between adjacent microlenses in the array leads to the excitation of collective modes, which destroy the phase synchronization between the microlenses [20, 21] and limit the operation range of the present device (supplementary information Movie 6). One possible strategy to extend the operation range to even higher frequencies is to place suitably designed obstacles that selectively suppress the hydrodynamic coupling between adjacent microlenses.

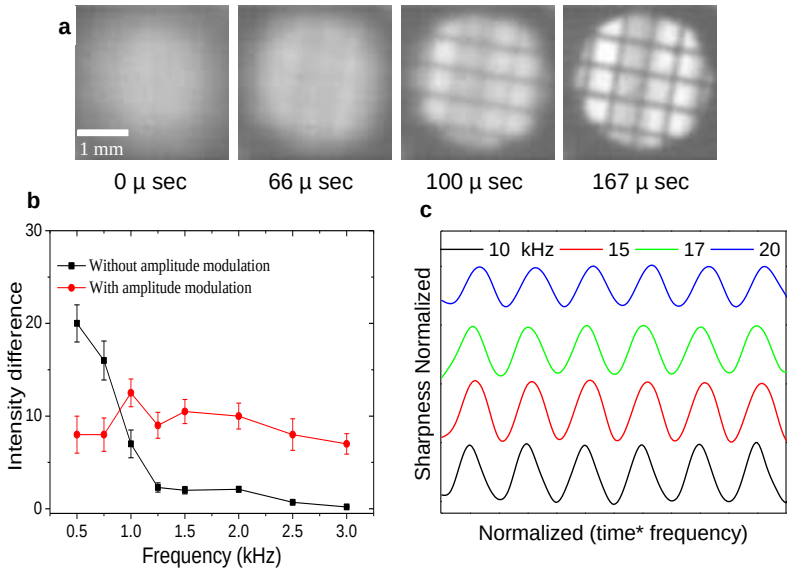

Fig. 5 High speed actuation of microlens. (a) Sequence of images acquired by the 200 µm aperture single microlens at 3 kHz in amplitude modulation mode. (b) Intensity variation vs. modulation frequency with conventional AC actuation (■) and with amplitude modulation of 10kHz carrier frequency (■). (c) Sharpness vs. normalized time (time x excitation frequency) for a single microlens with aperture diameter 75 µm for modulation frequencies of 10, 15, 17, 20 kHz (bottom to top) in amplitude modulation mode (carrier frequency 60 kHz).

5. Discussion

To turn the proof-of-concept experiment described here into a practical device it will be necessary to optimize the materials involved. In the first place, evaporation has to be suppressed by either switching to non-volatile liquids such as ethylene glycol and ionic liquids or – preferentially – by embedding the device in ambient oil. Overall, ambient oil will reduce the refractive power of the device due to the reduced contrast in refractive index. Note, however, that ambient oil usually leads to a higher Young's angle and to a wider tuning range of the contact angle. In

particular, the present device concept can be easily extended to a configuration where the contact angles on both the top and bottom side, i.e. θ_b and θ_t , decrease with increasing voltage. In this case, the lens can scan between being convex and being concave, which is not possible for most liquid lens designs. The increased range of contact angles and thus interface curvatures also allows to explore a wider range of materials (drop and ambient) than other EW lens designs at the same optical performance.

From a dynamic perspective, increases in viscosity and mass are likely to reduce the maximum operation frequency somewhat. Only in part, this will be compensated by the improved lubrication of the three-phase contact line in the presence of oil. To understand the dynamics of the device presented here and to explore its potential for non-scanning DC applications, it is useful to consider the physical phenomena governing the response of the liquid for a cylindrically symmetric device with a single aperture of radius a and a sandwiched reservoir drop or radius $R>>a>h$, where h is the plate spacing. The hydrodynamic resistance and the inertia of the sandwiched drop govern the transient behavior. Combining the time dependent Stokes equations for fluid flow and mass conservation we find two important results: first, both the viscous pressure drop ΔP_v and the inertial pressure drop ΔP_i between the edge of the sandwich drop and the aperture scale only logarithmically with the size of the reservoir but more strongly with plate spacing. For a lens operated at frequency ω, we find: $\Delta P_v=(3/4+\ln(R/a))(3\mu\omega a^4/h^3)Z$ and $\Delta P_i=(3/4+\ln(R/a))(\rho\omega^2 a^4/(16\gamma h))Z$, respectively, where Z is the vertical displacement of the meniscus. The logarithmic size dependence arises robustly from mass conservation arguments while the h^{-3} and h^{-1} scaling are a consequence of the channel flow. (This scaling is expected to prevail for more sophisticated hydrodynamic models.) These pressures should be compared with the Laplace pressure at the meniscus: $P_L = (4\gamma/a^2)Z$. Inserting parameter values we find at 100 Hz: $\Delta P_{v,i}/P_L = 0.01$. So, the pressure drop is smaller than the Laplace pressure but not negligible. In designing large arrays for high operating frequencies, it is thus advisable to reduce the viscous loss by increasing the plate spacing h. Second, from the expressions for the pressure drops we obtain the differential equation governing the meniscus motion. Its solution is given by: $Z(t) = Z_\infty(1-e^{-bt}\cos((\omega_o^2-b^2)^{1/2}t)$, where $b = 10\mu/\rho h^2$ is the damping coefficient and $\omega_o = [10\gamma h/\rho a^4]^{1/2}$ the resonance frequency of the meniscus motion. The transient time is now estimated as: $t_{trans} = \pi/\omega_o$ ~ 3 ms for the lens described in section 3. This suggest in DC operation switching frequencies up to 200 Hz. For the microlenses t_{trans} is one order of magnitude smaller. These estimates provide a reasonable scaling consistent with the overall lens performance. For a more detailed analysis of the hydrodynamic response of the device including in particular the excitation of higher eigenmodes on the lens surface, computational fluid dynamics calculations, adapting our recent work on oscillating sessile drops [22] to the geometry at hand, are in progress [23].

6. Conclusions

Our experiments demonstrate for the first time the successful operation of adaptive microlens arrays with operation frequencies in the kHz range. Figure. 1a-b shows the characteristic variation of the field of view and viewing angle obtained with the array from an object at a finite distance. Thanks to the tunability of the focal length sharp images can be generated with our arrays from objects at variable distances. Parallelization of microlenses into arrays allows for the reconstruction of three-dimensional image information due to the slightly different viewing angle of the images from each microlens [24][25]. Operating in reverse, the same microlens array should be useful for three-dimensional projection without need for specific viewing glasses. Furthermore, the design presented here has potential applications in various areas such as rapid parallel optical switches, artificial compound eye and tunable optical equipment such as Shack-Hartmann sensors.

Acknowledgement

We thank the Dutch Science Foundation NWO and the Foundation for Technical science STW for financial support within the VICI program.